Research Article | Vol. 28, No. 8 / 13 April 2020 / Optics Express 12080
Optics EXPRESS

Design of photonic crystal nonlinear laser power limiter based on topological edge states and optical Kerr effect

JIAN HUANG,[1,2] YUANGANG LU,[1,2,*] LANG ZHOU,[1,2] FENG XU,[3] AND DUNWEN ZUO[3]

[1] Key Laboratory of Space Photoelectric Detection and Perception of Ministry of Industry and Information Technology(College of Astronautics, Nanjing University of Aeronautics and Astronautics), Nanjing 210016, China
[2] College of Science, Nanjing University of Aeronautics and Astronautics, Nanjing 211106, China
[3] College of Mechanical and Electrical Engineering, Nanjing University of Aeronautics and Astronautics, Nanjing 210016, China
*luyg@nuaa.edu.cn

Abstract: We propose a novel topological photonic crystal nonlinear laser power limiter based on topological edge states and optical Kerr effect. In the proposed laser power limiter, a one-dimensional photonic crystal in topological edge state allows the relatively weak signal light with a certain wavelength to pass through with high transmission, but blocks most of the intense hostile or accidental laser with the same wavelength due to the change of topological edge state generated from optical Kerr effect. Taking a 1064 nm wavelength as an example, we have designed such a nonlinear laser power limiter corresponding to the wavelength. When the optical power density is low (less than 0.12 MW/cm^2), the light transmission can reach 82.54%, and the transmission can be reduced to 1.04% when the optical power density is increased to 11.66 MW/cm^2. Therefore, this method provides a new promising approach to realize laser protection at the desired wavelength.

1. Introduction

Because of the good characteristics of brightness, coherence, directionality and monochromaticity, lasers are commonly used in various fields such as industrial, medical and military applications. However, a high-energy laser beam usually produces irreversible damage to the human eyes and optical detectors. For example, a Q-switched laser is easy to achieve a high power density reaching the order of MW/cm^2. Therefore, it is necessary to find an effective laser power limiting method to avoid damage by the intense laser beams. In many cases, however, a weaker light is the useful signal expected to be detected and thus does not need to be attenuated. Hence, it is significant to design a nonlinear power limiter to allow the weak light pass through with a high transmission, while block the strong light with low transmission.

The main approaches of laser power limiting technology are based on linear optics [1–3], nonlinear optics [4–6] and thermal phase transition [7–9]. Among them, the protective materials based on the linear optical effect have the same light transmission for all the laser intensity, and cannot provide a high transmission for the weak light and a high attenuation for a strong light simultaneously. The typical laser protection material based on the principle of thermal phase transition is VO_2 film [10]. VO_2 film has a good application prospect because of its good thermal phase transition properties. However, it is very difficult to reduce the VO_2 phase transition temperature and the film response time to truly realize the rapid laser protection [11]. The laser protection technology based on optical nonlinearity overcomes the shortcomings of the linear optical protection method [12,13] and can realize the intelligent protection with the

#390297 https://doi.org/10.1364/OE.390297
Journal © 2020 Received 12 Feb 2020; revised 30 Mar 2020; accepted 30 Mar 2020; published 8 Apr 2020

Optics EXPRESS

properties of high transmission for the weak light and high attenuation for the strong light [14]. The nonlinear protection technology generally depends on the nonlinear optical effects of the constituent materials, including nonlinear absorption, nonlinear refraction, nonlinear reflection and nonlinear scattering [15]. The nonlinear absorption effects include the reverse saturable absorption and two-photon absorption. In materials the reverse saturable absorption can enhance the absorption of light with the increasing light intensity, and thus is a good mechanism for laser power limiting [16]. While for the two-photon absorption, the absorption coefficient is generally small, and thus restricts its application in laser power limiting [17]. For the power limiting techniques driven by nonlinear reflection, most incident radiation can be reflected and thus can avoid the power limiter to be destroyed by the high power laser [18,19]. However, the nonlinear reflective methods have an obvious drawback, which is the requirements of special incident angles [20]. In protection techniques based on nonlinear scattering, the scatter generated from non-uniform distribution of the liquid solution under strong light is used to achieve the laser power limiting [21]. However, the optical limiting efficiency is degraded when the temperature of the suspension increases due to the high light intensity [22].

In this paper we innovatively propose a topological photonic crystal nonlinear laser power limiter based on topological edge states (TES) and optical Kerr effect. The TES is a state in which photons can be induced to transmit through the photonic crystal at frequencies in the bandgap, which offers a new way to control photons transportation [23]. The TES can protect the transmission of photons from the effects of scattering by impurities and defects in materials, and the design based on the third order nonlinear effect enables the optical power limiter to protect against pulsed laser irradiance in nanoseconds regime. In addition, because of the less sensitivity of the incident light's angles, the proposed structure has more applications in power limiting than traditional thin film stacks [24]. Therefore, we envisage the realization of high transmission or blocking of light by controlling the existence or disappearance of the TES. There are many methods for constructing TES. Among them, it is a convenient way to design the TES by controlling the band structure of photonic crystals. In nonlinear optical materials, the light intensity will change the refractive index of the medium and the corresponding band structure [25]. Therefore, through reasonable design, the laser power limiter can control the existence or disappearance of the TES according to the change of the light intensity, and thus realize the self-activated limiting of the light. Taking the 1064 nm wavelength as an example, the laser power limiter we designed is effective to protect optical sensors, human eyes, and other sensitive components. The layered film structure we proposed is relatively simple to fabricate. Compared with the nonlinear limiting structures of gas and liquid, the proposed structure is layered films and insensitivity to external environment. Our approach can be better applied to laser goggles, optical sensor protection and a compact and efficient integrated optical limiter.

2. Principle

We propose a one-dimensional photonic crystal power limiter to construct the TES. The TES generated in the photonic crystal is used to ensure photons transmission and obtain relatively high transmission at low power density. Because of the optical Kerr effect, the refractive index n of the photonic crystal changes as the incident light power increases. With a specific design, the band gap of photonic crystals narrows as the optical power density increases, limiting the transmission of light. When the incident optical power density continues to increase, the band structure no longer meets the conditions of the TES. In such cases, the photonic crystal returns to its original forbidden band state, preventing light with a certain wavelength from passing through to achieve the purpose of light power limiting.

The proposed one-dimensional photonic crystal power limiter is shown in Fig. 1. The nonlinear photonic crystal limiter is composed of a nonlinear photonic crystal L (PC_L) and a linear photonic crystal R (PC_R). It consists of four materials that are periodically arranged. The

Optics EXPRESS

PC_L includes two nonlinear materials *A* and *B*, and the *PC_R* includes two linear materials *C* and *D*. The thickness of layer *A*, *B*, *C* and *D* is d_A, d_B, d_C and d_D, respectively. There are six sandwich-like unit cells $A_{0.5}BA_{0.5}$ make up the whole *PC_L* and the unit cell is marked with a red dotted rectangle box. In each unit cell, a layer *B* is sandwiched in the middle of two halves of layer *A*. The subscript 0.5 represents half of a complete layer *A*. The similar six sandwich-like unit cells $C_{0.5}DC_{0.5}$ are arranged in *PC_R*, where a layer *D* is sandwiched in the middle of two halves of layer *C* in each unit cell.

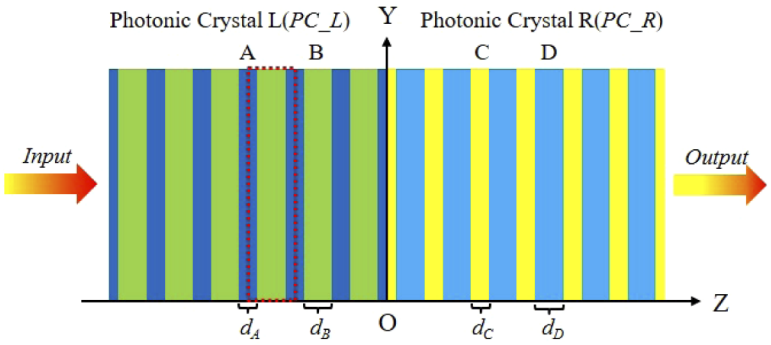

Fig. 1. The structure of a one-dimensional photonic crystal laser power limiter. The photonic crystal *L* (*PC_L*) includes two nonlinear materials *A* and *B*, and the photonic crystal *R* (*PC_R*) includes two linear materials *C* and *D*.

By designing a suitable linear index of refraction for the power limiter, the TES of the power limiter appears at low light power density, causing the appearance of a transmission peak at the position where the photonic crystal is originally forbidden. This means the light that could not be passed originally can achieve high transmission in this state. As the optical power density increases, the refractive index of the nonlinear portion of the photonic crystal changes due to the optical Kerr effect, i.e. $n(I)= n_0+n_2 \cdot I$, where n_0 is the linear refractive index of the nonlinear material, n_2 is nonlinear-index coefficient of the nonlinear material and I is incident light intensity. As a result, the position of the transmitted peak will be restored to the forbidden band again, preventing the light from passing through the limiter. The center frequency of the band gap ω_{m_L} and ω_{m_R} of the *PC_L* and *PC_R* can be calculated by the relation [26]

$$\begin{aligned} \omega_{m\_L} &= m\pi c/(n_a d_a + n_b d_b), \\ \omega_{m\_R} &= m\pi c/(n_c d_c + n_d d_d), \end{aligned} \tag{1}$$

where c represents the speed of light in vacuum, m is a positive integer, n_a, n_b, n_c and n_d represent the refractive indices of the media *A*, *B*, *C* and *D*, respectively. When the four media are determined, we can adjust the thicknesses of the unit layers to make both of the center frequencies ω_{m_L} and ω_{m_R} close to the corresponding wavelength λ to be limited.

In order to allow the useful weak signal light to pass through the power limiter, we need to generate the TES at the desired wavelength λ by adjusting the parameters of *PC_L* and *PC_R*. The TES of a one-dimensional photonic crystal can be simply thought to be related to the Zak phase, which can be calculated by [27]

$$\theta_n^{Zak} = \int_{-\pi/\Lambda}^{\pi/\Lambda} [i \int_{unitcell} \varepsilon(z) u_{n,q}^*(z) \partial_q u_{n,q}(z) dz]\, dq, \tag{2}$$

where Λ is the length of the complete unit cell constituting the photonic crystal, $\varepsilon(z)$ denotes the function of permittivity, $u_{n,q}(z)$ is the Bloch electric field eigenfunction of the *n—th* band

Optics EXPRESS

with a Bloch wave vector q. For such a 1-D photonic crystal, $u_{n,q}(z)$ can be calculated by the transmission matrix method [28]. In particular, for a 1-D mirror system, the Zak phase can be quantized at either 0 or π [29]. The topological symmetry of *n-th* gap can be determined from the sum of the Zak phases, θ^{Zak}, of all the bands below it, and we calculate sign of the topological properties [26] of *PC_L* and *PC_R* by using

$$\mathrm{sgn}[(-1)^n \exp(\sum_{m=0}^{n-1} \theta_m^{Zak})], \tag{3}$$

where θ_m^{Zak} is the Zak phase of the *m—th* band of photonic crystal and sgn is the sign function. If the sign of the topological properties of *PC_L* and *PC_R* are respectively denoted as $\mathrm{sgn}(\mathrm{TP}_{PC\_L})$ and $\mathrm{sgn}(\mathrm{TP}_{PC\_R})$, and neither of the band gap of *PC_L* and *PC_R* is zero, the existing condition [25] of the TES of the power limiter can be described as $\mathrm{sgn}(\mathrm{TP}_{PC\_L})+\mathrm{sgn}(\mathrm{TP}_{PC\_R}) = 0$. In addition, the Zak phase of the lowest *0—th* band of the *PC_L* ($\theta_{0\_L}^{Zak}$) or *PC_R* ($\theta_{0\_R}^{Zak}$) can be determined by the sign of [1-$\varepsilon_a\mu_b/\varepsilon_b\mu_a$] or [1-$\varepsilon_c\mu_d/\varepsilon_d\mu_c$] [26], i.e.

$$\begin{aligned} \exp(i\theta_{0\_L}^{Zak}) &= \mathrm{sgn}[1 - \varepsilon_a\mu_b/\varepsilon_b\mu_a], \\ \exp(i\theta_{0\_\mathrm{R}}^{Zak}) &= \mathrm{sgn}[1 - \varepsilon_\mathrm{c}\mu_\mathrm{d}/\varepsilon_\mathrm{d}\mu_\mathrm{c}], \end{aligned} \tag{4}$$

where ε_a, ε_b, ε_c, ε_d, μ_a, μ_b, μ_c and μ_d are the dielectric constant and permeability of media *A*, *B*, *C* and *D*, respectively. Once the TES is formed, incident light with the wavelength of λ can achieve high transmission at low power.

Next, we use the schematic diagrams in Fig. 2 to further clarify the principle of nonlinear laser power limiter based on topological edge states and optical Kerr effect. The periodic structure frequency ω and Bloch wave vector K of a one-dimensional photonic crystal satisfy the dispersion relationship

$$\omega_\pm^2 = \frac{K^2}{\mu(\varepsilon_0 \pm |\varepsilon_1|)}, \tag{5}$$

where $\omega_\pm$ are the spectral band edges, μ is the permeability tensor, ε_0 and ε_1 are the zeroth and first Fourier component of the dielectric tensor, respectively. Taking the unit cell $A_{0.5}BA_{0.5}$ and $C_{0.5}DC_{0.5}$ of *PC_L* and *PC_R* as examples, we calculated their band structures at different optical power density, as shown in the first and second columns of Fig. 2. And the corresponding transmission is shown in the last column of Fig. 2. The rectangles in the figure represent the band gap, and the positive and negative signs of the topological properties are corresponding to the red and blue color of the rectangles, respectively.

The $\mathrm{sgn}(\mathrm{TP}_{PC\_L})$ and $\mathrm{sgn}(\mathrm{TP}_{PC\_R})$ are opposite when the input optical power density is low. In such cases, the center position of the band gap ($0.5\mathrm{v}_0$ corresponds to $2\lambda_0$) appears a TES, inducing photons to transmit through the photonic crystals at frequencies within the bandgap. For linear optical materials, their third-order nonlinear coefficients are too small to make their dielectric constant and permeability change with the increasing incident power density. In the proposed design, the *PC_R* is composed of two linear optical materials. Therefore, the band structure of *PC_R* can remain unchanged with the increasing incident optical power, as shown in Fig. 2. However, the band gap of *PC_L* gradually narrows as the input power density increases because the *PC_L* consists of two optical nonlinear materials *A* and *B*, which results in the gradual decrease of the light transmission to achieve the purpose of optical limiting. As the input power density continues to increase, the two bands around the gap of *PC_L* are reversed, and the sign of the topological property changes from positive to negative. In such cases, the topological properties of *PC_L* and *PC_R* are the same and the TES disappears, and the original bandgap state can still play the role of power limiting. The specific relationship between the band gap width of *PC_L* and the input optical power density is shown in Fig. 3. The red area in the left part indicates that $\theta_0^{Zak} = \pi$, and the topological property of the band gap is positive. In contrast,

Optics EXPRESS

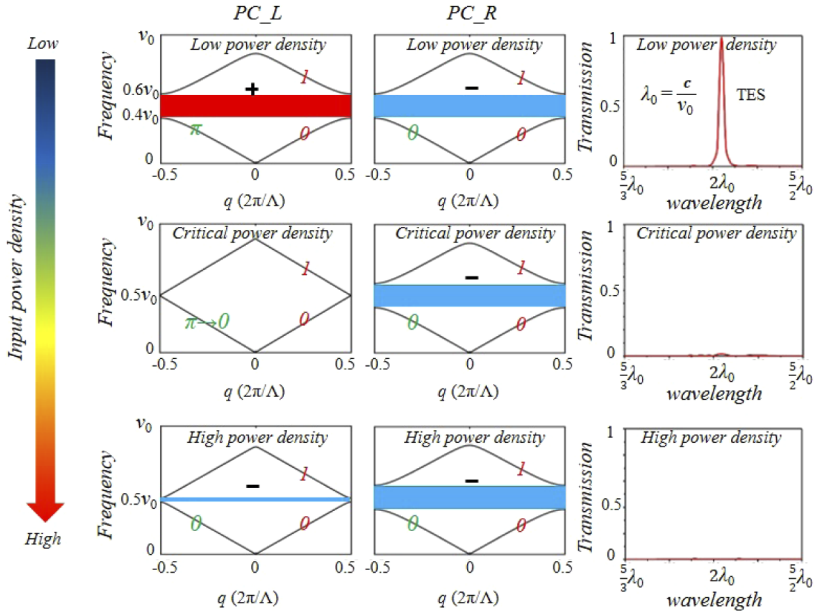

Fig. 2. The schematic diagrams of the nonlinear laser power limiter based on topological edge states and optical Kerr effect. The change of the band structure and transmission curve of the photonic crystal with the increase of the incident light power density. The Zak phase of each individual band is represented by a green number (*0* or π), and the numbers of the bands are listed with red labels (0 and 1). The positive and negative signs of the topological properties are corresponding to the red and blue color of the rectangles, respectively.

the blue area in the right part indicates that $\theta_0^{Zak} = 0$, and the sign of the topological properties of the band gap is negative.

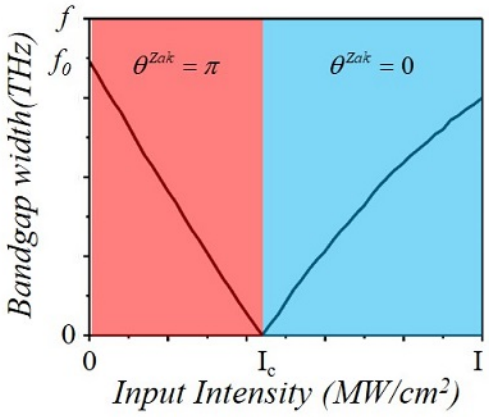

Fig. 3. The trend of *PC_L*'s bandgap width with increasing input optical intensity. The f_0 is the band gap width of the initial structure, and I_C is the critical power density where the topological property of the bandgap changes from π to *0*.

Optics EXPRESS

3. Structure and material properties of nonlinear laser power limiter

Taking the 1064 nm wavelength as an example, we used this new method to design the optical limiter. As shown in Fig. 1, the *PC_L* is composed of two Kerr nonlinear materials *A* and *B*, and the *PC_R* is composed of two linear materials *C* and *D*. The periodic unit cell for *PC_L* is $A_{0.5}BA_{0.5}$. The parameters of Kerr nonlinear media *A* and *B* are as follows: n_A=2.40, n_B=1.59, d_A=111 nm and d_B=158 nm. Similar to the *PC_L*, the unit cell of the *PC_R* is $C_{0.5}DC_{0.5}$. The parameters of media *C* and *D* are as follows: n_C=1.48, n_D=2.29, d_C=169 nm and d_D=115 nm. Each photonic crystal consists of six unit cells of $A_{0.5}BA_{0.5}$ and $C_{0.5}DC_{0.5}$, respectively. The nonlinear refractive index of medium *A* is $n_{2A}=2.10\times10^{-8}$ cm^2/W, and the nonlinear refractive index of medium *B* is $n_{2B}=-1.84\times10^{-8}$ cm^2/W. To meet the refractive index requirement, we choose nano-Au:(nano-Fe:$BaTiO_3$) [30] as the material of medium *A*, and Sn doped ZnO thin films with 1% doping concentration (1% Sn-ZnO) [31] as the material of medium *B*. The absorption coefficient α and laser damage threshold I_{thr} of the substrate materials of medium *A* and *B* are α_A=0.02 cm^{-1} [32], α_B=5.03 cm^{-1} [31], I_{thr_A}=0.54 GW/cm^2 [33] and I_{thr_B}=1.06 GW/cm^2 [34], respectively. In addition, we chose PMMA and ZnS as materials for linear media *C* and *D* to meet linear refractive index requirements. The nonlinear refractive index of materials *C* and *D* are $n_{2C}=5.78\times10^{-11}$ cm^2/W [35] and $n_{2D}=5.76\times10^{-19}$ cm^2/W [36], respectively. The absorption coefficients of materials *C* and *D* are 0.15 cm^{-1} [37] and 0.25 cm^{-1} [38], and their laser damage thresholds are 2.63 GW/cm^2 [39] and 0.34 GW/cm^2 [40], respectively. The parameters of the four materials are shown in Table 1.

Table 1. Related parameters of the four materials.

Medium	Thickness d(nm)	Linear refractive index n_0	Nonlinear refractive index coefficient n_2(cm^2/W)	Absorption coefficient α(cm^{-1})	Laser damage threshold I_{thr}(GW/cm^2)
A(nano-Au:(nano-Fe:$BaTiO_3$))	111	2.40	2.10×10^{-8}	0.02	0.54
B(1% Sn-ZnO)	158	1.59	-1.84×10^{-8}	5.03	1.06
C(PMMA)	169	1.48	5.78×10^{-11}	0.15	2.63
D(ZnS)	115	2.29	5.76×10^{-19}	0.25	0.34

4. Results and discussion

In order to effectively block the incident laser at the wavelength of 1064 nm, the wide photonic band gaps of *PC_L* and *PC_R* around 1064 nm are necessary. Firstly, we separately calculate the transmission spectra of *PC_L* and *PC_R* at the laser wavelength from 800 to 1300 nm under low light condition (0.12 MW/cm^2) by finite element analysis software, and the results are shown in Fig. 4(a). It should be noted that, for the transmission curves we obtained in the range from 800 to 1300 nm, the refractive indexes of the four materials used in the calculation are the refractive indexes corresponding to the wavelength of 1064 nm. Since the linear refractive index changes of these four materials are small within the near-infrared wavelength range of 800~1300 nm, the calculation results in Fig. 4 are reliable. We can see that the photonic band gap of the *PC_L* is in the range of 900~1100 nm and that of the *PC_R* is in the range of 1000~1150 nm. There is an overlap (1000 nm-1100 nm) between the band gaps of these two photonic crystals, which meets the design requirements for laser power limiting at 1064 nm with high power density.

The reason why the overlap section appears is that the optical path lengths of the smallest periodic unit cell in them are approximated, i.e. $n_A\cdot d_A+n_B\cdot d_B=n_C\cdot d_C+n_D\cdot d_D$. Next, we construct a TES at the interface between the *PC_L* and the *PC_R* to ensure that a weaker signal light can pass through. By calculating the transmission spectrum of the entire limiter in the range of

Optics EXPRESS

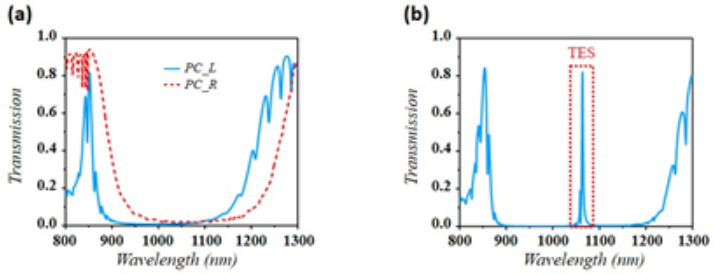

Fig. 4. (a) The transmission curves of the *PC_L* and *PC_R* in the range of 800~1300 nm. The forbidden bands of the *PC_L* and the *PC_R* overlap around 1064 nm. (b) The transmission spectrum of the entire laser power limiter in the range of 800~1300 nm.

800~1300 nm, it can be seen that the TES we want to obtain appears at 1064 nm, as shown in Fig. 4 (b). The red dotted rectangle marks a transmission peak at 1064 nm due to the TES.

Next, we consider the changes in the limiting structure during the process of increasing light intensity. In the case of weaker light intensity, the 1064 nm laser can be successfully transmitted the limiting structure by the TES. As the light intensity increases, the effective refractive indices of materials *A* and *B* vary with the change of power density of incident laser driven by optical Kerr effect. As shown in Fig. 5, we calculated the refractive index of the photonic crystal power limiter at low optical power density (0.12 MW/cm^2) and high optical power density (11.66 MW/cm^2). The blue dotted line and the red solid line represent the refractive index distribution of the power limiter at low and high optical power density, respectively. It shows that the refractive index of the nonlinear materials of *PC_L* change significantly at high optical power density. The change in refractive indices is inhomogeneous due to the inhomogeneous distribution of light field. Because of the difference in the nonlinear refractive index coefficients n_2, the refractive indices of layers *A* and *B* increase and decrease, respectively.

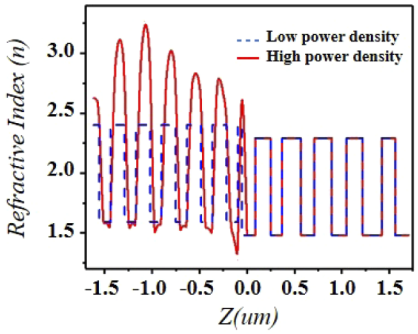

Fig. 5. The refractive index distribution of the photonic crystal power limiter at low and high optical power density The parts of $Z < 0$ and $Z > 0$ are corresponding to the *PC_L* and *PC_R*, respectively.

The change of the effective refractive index due to Kerr effect causes the photonic crystal band properties to change, resulting in the gradual disappearance of the TES. Then we compute the optical limiting effect of the structure by finite element analysis. Considering the incident light entering vertically from the left side of the limiter, we calculate the electric field distribution of the nonlinear limiter for a laser with a wavelength of 1064 nm in the conditions of weak light (0.12 MW/cm^2) and strong light (11.66 MW/cm^2), as shown in the Fig. 6(a). The green area on the left is corresponding to the *PC_L*, and the yellow area on the right is corresponding to the

Optics EXPRESS

PC_R. The black solid curve represents the electric field distribution under low light conditions, indicating that a TES exists at the interface between the *PC_L* and *PC_R*. The red dotted curve represents the distribution of the electric field under strong light, and it can be seen that the TES almost disappears in this case. It is obvious that the strong light is well limited from the electric field distribution diagram. In the proposed structure, we practically make the absolute value of the d_B/d_A to be the same with n_{2A}/n_{2B}. This allows the effective optical path length $n_A \cdot d_A + n_B \cdot d_B$ to be constant with the same intensity of light, thereby ensuring that the position of the transmission peak of the structure does not change. We continuously added the incident optical power density and the transmission peak decreased accordingly, as shown in Fig. 6(b). In order to obtain the transmission curves in the wavelength range from 1060 nm to 1074 nm, the refractive indexes and nonlinear refractive index coefficients of the four materials used in the calculation are that of corresponding to the wavelength of 1064 nm. As the changes of refractive indexes and nonlinear refractive index coefficients of the four materials are small within the narrow wavelength range from 1060 nm to 1074 nm, the obtained transmission curves have high reliability. Each of the transmission curves in Fig. 6(b) is obtained by sweeping the laser wavelength while keeping the laser power. The value of the maximum power density we applied is much lower than the laser damage threshold of the four materials, and thus a desired limiting effect can be achieved. The optical limiting threshold, one of the parameters to describe the performance of optical power limiter, is defined as the incident intensity where the transmission drops to 50% of the initial linear value [41]. The optical limiting threshold of the structure is found to be 0.31 MW/cm^2. The value is lower than some other nonlinear materials such as C_{60}, porphyrins, and phthalocyanines [42–44], and thus shows that this structure has better power limiting sensitivity.

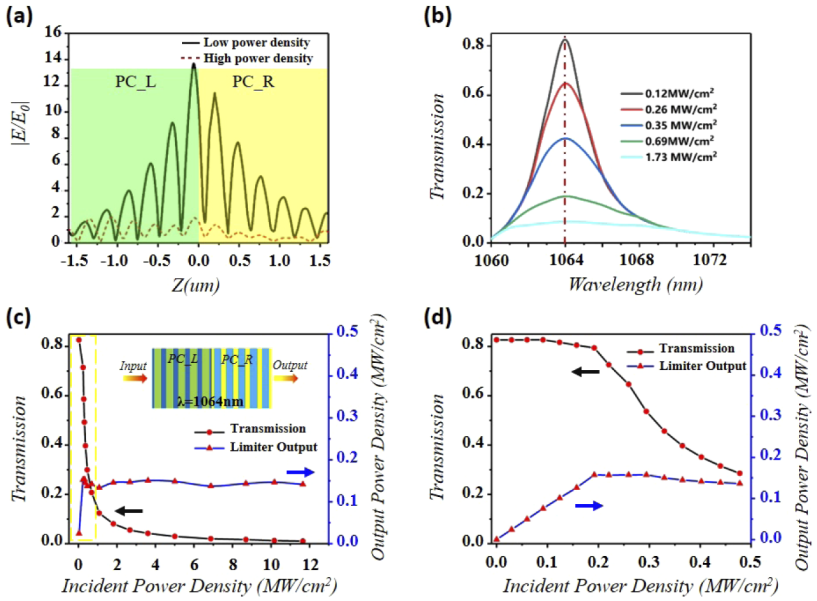

Fig. 6. (a) The electric field distribution of the photonic crystal power limiter at low and high optical power densities. (b) Five transmission spectrum of optical limiter with input power *density* increased from 0.12 MW/cm^2 to 1.73 MW/cm^2. (c) The transmission and output power density curves as the incident intensity increases from 0.12 MW/cm^2 to 11.66 MW/cm^2. (d) An enlarged plot of the transmission and output power density when I_{input}<0.5 MW/cm^2, which is marked by the yellow dotted box in Fig. 6(c).

Optics EXPRESS

We also calculated the transmission with different light power densities at incident wavelengths of 1064 nm. The optical transmission and output power density versus incident intensity is shown in Fig. 6(c). The Fig. 6(d) is an enlarged plot of the transmission and output power density when the incident power density is less than 0.5 MW/cm^2, which is marked by the yellow dotted box in Fig. 6(c). The blue line with red triangle represents the output power density after passing through this optical limiter, and the black line with red circle is the transmission corresponding to the incident optical power density. The trend of the proposed limiter output is very close to the response of the ideal optical limiter proposed in the Ref. [45]. It can be seen that the transmission decreases rapidly from 82.54% to 1.04% as the incident power density increases from 0.12 MW/cm^2 to 11.66 MW/cm^2. The output power density talso increases linearly with the input power density (I_{input}<0.2 MW/cm^2), and finally the value is stable around 0.14 MW/cm^2, which is a low output power density that one would expect from a good power limiter [46]. The results show that the laser power limiter we designed has a good protection effect on the 1064 nm laser. The method of finite element analysis has been used for analyzing optical limiters [24,47]. The comparison with the results of laser power limiter reported in recent years is shown in Table 2. The optical limiter we designed shows a good performance in laser power limiting. Compared with most power limiting methods, the proposed power limiter possesses higher linear transmission. Simultaneously, the transmission of the power limiter under strong light (11.66 MW/cm^2) can be reduced to 1.04%. Although the limiting method based on phase change materials has better performance [20], the photothermal effect induced phase change requires much longer time and cannot respond quickly to narrow laser pulses. In contrast, the proposed power limiter based on TES and the optical Kerr effect has a good limiting effect on nanoseconds pulses [24].

Table 2. The effect of several limiting methods.

The limiting methods	Transmission under weak light(T_1)	Transmission under strong light(T_2)	Laser damage threshold I_{thr}(GW/cm^2)	The on-set threshold (MW/cm^2)	Reference
Nonlinear laser power limiter based on topological edge states	82.54%	1.04%	0.34	0.12	This paper
Reflective nonlinear photonic structure	42%	2.4%	7.39×10^{-9}	–	[18]
Reflective optical limiter using GST phase change material	85%	0.02%	–	–	[20]
2D nonlinear photonic crystals	–	–	0.89	9	[24]
Optical limiter using epsilon-near-zero grating	55%	almost 0%	–	–	[47]
Photonic crystal limiter embedded in an absorbing defect layer	60%	14%	23.4(peak input power)	–	[48]

5. Fabrication feasibility and tolerance analysis

Compared to the complicated and difficult fabrication process of two-dimensional, three-dimensional photonic crystal, one-dimensional photonic crystals can be easily realized by various mature fabrication processes [49]. The existing technology can easily prepare a nano-scale photonic crystal film, making the fabrication of the power limiter possible. For example, some works have prepared ZnO films by atomic layer deposition where the surface roughness value can reach 0.12 nm [50]. Some researchers have prepared PMMA nano-films with a surface roughness of 0.14 ± 0.01 nm [51]. In another work, researchers have prepared SiO_2/TiO_2 one-dimensional photonic crystals by sol-gel method, and the root mean square deviation of SiO_2 film is 0.346 nm

Optics EXPRESS

[52]. It can be seen that different types of films and different fabrication processes result in different values of surface roughness. Considering the possible surface roughness of the fabrication process, we further analyze the effect of surface roughness on the limiting effect of the structure with the low power density incident light of 1064 nm. Practically, compared with the theoretical thickness of each layer, we assume the deviation thickness of each media layer in the power limiter changes from −0.5 nm to 0.5 nm while fixing the thickness of other dielectric layers. By alternately changing the thickness of media A, B, C and D while keeping the thickness of other dielectric layers, we calculated the transmission with the incident intensity of 0.12 MW/cm^2. The values of transmissions are shown in Fig. 7(a). The curves of the four colors of purple, green, dark blue, and light blue indicate the effects of the surface roughness of the media *A*, *B*, *C*, and *D* on the light transmission at 1064 nm, respectively.

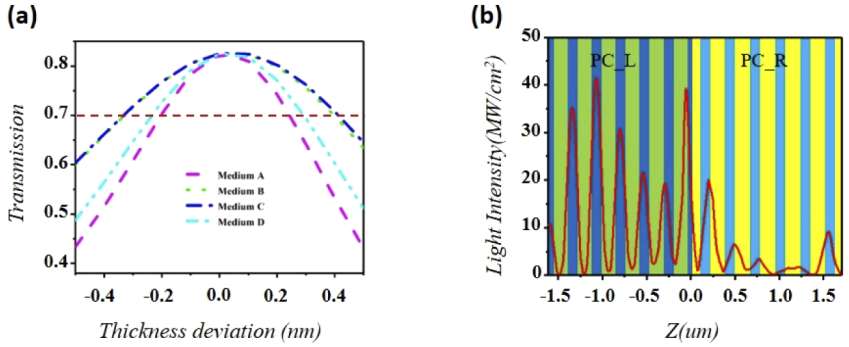

Fig. 7. (a) The transmission curve of the 1064 nm laser with weak light (0.12 MW/cm^2) caused by the surface roughness of the limiting structure medium. (b) Light intensity distribution inside the power limiter with an incident optical power density of 11.66 MW/cm^2.

It can be seen that the value of light transmissions at 1064 nm are lowered with the increasing absolute value of deviation thickness, which can be explained by the above formula (1). The surface roughness of the dielectric layer causes the position of the peak of the transmission deviate from 1064 nm. In order to ensure a high transmission of 1064 nm signal light or probe light, we use 70% transmission as the minimum standard to consider the allowable surface roughness of each medium. The allowable surface roughness of the medium *A*, *B*, *C* and *D* are 0.45, 0.75, 0.75 and 0.55 nm, respectively. The allowable surface roughness of each medium layer can be fabricated using modern technology in References of [50–52].

In addition, we also considered the influence of heating due to the linear light absorption in the materials during the process of the laser power limiting. We calculated the light intensity distribution inside the power limiter with an incident optical power density of 11.66 MW/cm^2, as shown in Fig. 7(b). The maximum light intensities corresponding to the media A, B, C, and D are 41.37, 17.34, 18.11, and 20.01 MW/cm^2, respectively. According to Beer-Lambert law, which is $I = I_0 e^{-\alpha L}$ (I and I_0 are respectively the output and input light intensity of the media, α is absorption coefficient, and L is the thickness of the media), we calculate the light energy absorbed by the materials. For composite materials A and B, we mainly consider the influence of the substrate materials $BaTiO_3$ and ZnO. The related optical and thermal parameters of the four materials are listed in the Table 3 [53–55]. Therefore, we can obtain the temperature change ΔT of each medium by

$$\Delta T = \frac{Q}{Cm} = \frac{\Delta I \tau}{C \rho l}, \tag{6}$$

Optics EXPRESS

where ΔI is the absorbed light intensity, τ is the laser pulse width, C is the specific heat capacity and ρ is density of the materials. In order to fully consider the influence due to the heat generated from light absorption inside the medium, we take the effective lengths l as that corresponding to 90% of the maximum light intensity of the four media. According to the light field distribution obtained by using finite element analysis, the effective lengths l of the media A, B, C and D are 45, 5, 5 and 37 nm, respectively. We use the region with the largest thermal expansion to estimate the deformation of the entire power limiter due to photothermal effect. We obtain the thickness change ΔL of the four media by the thermal expansion formula $\Delta L=\beta L\Delta T$, where β is coefficient of thermal expansion. When the incident optical power density reaches 11.66 MW/cm^2 and the pulse width is 10 ns, the thickness changes of the media A, B, C and D are 1.27×10^{-6}, 2.20×10^{-2}, 5.50×10^{-3} and 4.95×10^{-4} nm, respectively. Since these thickness changes are so small and thus can be neglected, the influence of the heat generated from light absorption on the performances of the power limiter can be omitted.

Table 3. Optical and thermal properties of the four materials.

Medium	Absorption coefficient α(cm^{-1})	Density ρ(g/cm^3)	Specific heat capacity C(J/kg˙K)	Coefficient of thermal expansion β(k^{-1})	Thickness changes ΔL(nm)
A($BaTiO_3$)	0.02	6.02	527	6.50×10^{-6}	1.27×10^{-6}
B(ZnO)	5.03	5.68	520	1.48×10^{-5}	2.20×10^{-2}
C(PMMA)	0.15	1.18	1464	6.14×10^{-5}	5.50×10^{-3}
D(ZnS)	0.25	4.09	469	2.57×10^{-5}	4.95×10^{-4}

6. Conclusion

In conclusion, combining the TES of the photonic crystal structure and the nonlinear optical Kerr effect, we propose a novel photonic crystal nonlinear laser power limiter. The limiter can allow weak signal light to pass through with high transmission at a certain wavelength, but blocks most of the intense hostile or accidental laser with the same wavelength. Taking the 1064 nm wavelength as an example, the transmission of the proposed limiter can reach 82.54% when a weak incident optical intensity is less than 0.12 MW/cm^2, and the transmission can be reduced to 1.04% when the incident intensity reaches 11.66 MW/cm^2. In addition, combined with the existing fabrication process, we analyze the effect of surface roughness on the limiter and give the allowable surface roughness of each medium. We also consider the influence of heating due to the light absorption in the power limiter, and the calculation results show that it is too small and thus can be omitted. Our work provides a new approach to design high-performance nonlinear laser power limiter.

Funding

National Natural Science Foundation of China (61875086, 61377086); Aerospace Science Foundation of China (2016ZD52042).

Disclosures

The authors declare no conflicts of interest.

References

1. T. Kololuoma, J. A. I. Oksanen, P. Raerinne, and J. T. Rantala, "Dye-doped sol-gel coatings for near-infrared laser protection," J. Mater. Res. **16**(8), 2186–2188 (2001).
2. M. Chen, C. Li, M. Xu, W. Wang, S. Ma, and Y. Xia, "Eye-protection glasses against YAG laser injury based on the band gap reflection of one-dimensional photonic crystal," Opt. Laser Technol. **39**(1), 214–218 (2007).

Optics EXPRESS

3. Z. W. Guan, J. Li, T. Zhang, Y. Z. Zhang, P. R. Liu, and Z. Y. Wang, "An Organic Double-Layer Coating on Aluminum and Steel Substrates for Anti-Laser Protection," Mater. Sci. Forum **815**, 690–694 (2015).
4. Q. Li, C. Liu, Z. Liu, and Q. Gong, "Broadband optical limiting and two-photon absorption properties of colloidal GaAs nanocrystals," Opt. Express **13**(6), 1833–1838 (2005).
5. Q. Gan, S. Li, F. Morlet-Savary, S. Wang, S. Shen, H. Xu, and G. Yang, "Photophysical properties and optical limiting property of a soluble chloroaluminum-phthalocyanine," Opt. Express **13**(14), 5424 (2005).
6. C. P. Singh, K. S. Bindra, G. M. Bhalerao, and S. M. Oak, "Investigation of optical limiting in iron oxide nanoparticles," Opt. Express **16**(12), 8440 (2008).
7. Y. Dachuan, X. Niankan, Z. Jingyu, and Z. Xiulin, "Vanadium dioxide films with good electrical switching property," J. Phys. D: Appl. Phys. **29**(4), 1051–1057 (1996).
8. I. P. Parkin and T. D. Manning, "Intelligent Thermochromic Windows," J. Chem. Educ. **83**(3), 393 (2006).
9. W. Wang, Y. Luo, D. Zhang, and F. Luo, "Dynamic optical limiting experiments on vanadium dioxide and vanadium pentoxide thin films irradiated by a laser beam," Appl. Opt. **45**(14), 3378 (2006).
10. S. Chen, H. Ma, X. Yi, T. Xiong, H. Wang, and C. Ke, "Smart VO_2 thin film for protection of sensitive infrared detectors from strong laser radiation," Sens. Actuators, A **115**(1), 28–31 (2004).
11. S. Wang, M. Liu, L. Kong, Y. Long, X. Jiang, and A. Yu, "Recent progress in VO_2 smart coatings: Strategies to improve the thermochromic properties," Prog. Mater. Sci. **81**, 1–54 (2016).
12. D. Yan-qiu, "Laser Protection Materials against Optical Intensity and Protection Mechanism," *2010 Symposium on Photonics and Optoelectronics* (IEEE, 2010), pp. 1–4
13. G. Ritt, S. Dengler, and B. Eberle, "Protection of optical systems against laser radiation," Proc. SPIE **7481**, 74810U (2009).
14. J. M. Hales, M. Cozzuol, T. E. Screen, H. L. Anderson, and J. W. Perry, "Metalloporphyrin polymer with temporally agile, broadband nonlinear absorption for optical limiting in the near infrared," Opt. Express **17**(21), 18478–18488 (2009).
15. Wang and Ling, "Self-activating liquid crystal devices for smart laser protection," Liq. Cryst. **43**(13-15), 2062–2078 (2016).
16. J. S. Shirk, "Protecting the War Fighter's Vision In a Laser-Rich, Battlefield Environment," Opt. Photonics News **11**(4), 19 (2000).
17. L. Zhang and L. Wang, "Recent research progress on optical limiting property of materials based on phthalocyanine, its derivatives, and carbon nanotubes," J. Mater. Sci. **43**(17), 5692–5701 (2008).
18. E. Makri, T. Kottos, and I. Vitebskiy, "Reflective optical limiter based on resonant transmission," Phys. Rev. A **91**(4), 043838 (2015).
19. J. H. Vella, J. H. Goldsmith, A. T. Browning, N. I. Limberopoulos, I. Vitebskiy, E. Makri, and T. Kottos, "Experimental Realization of a Reflective Optical Limiter," Phys. Rev. Appl. **5**(6), 064010 (2016).
20. A. Sarangan, J. Duran, V. Vasilyev, N. Limberopoulos, I. Vitebskiy, and I. Anisimov, "Broadband Reflective Optical Limiter Using GST Phase Change Material," IEEE Photonics J. **10**(2), 1–9 (2018).
21. X. Sun, Y. Xiong, P. Chen, J. Lin, W. Ji, J. H. Lim, S. S. Yang, D. J. Hagan, and E. W. Van Stryland, "Investigation of an optical limiting mechanism in multiwalled carbon nanotubes," Appl. Opt. **39**(12), 1998–2001 (2000).
22. Y. Hyojung and K. Sokwon, "Temperature Effects in an Optical Limiter Using Carbon Nanotube Suspensions," J. Korean Phys. Soc. **47**(4), 610–614 (2005).
23. C. Li, X. Hu, W. Gao, Y. Ao, S. Chu, H. Yang, and Q. Gong, "Thermo-optical Tunable Ultracompact Chip-Integrated 1D Photonic Topological Insulator," Adv. Opt. Mater. **6**(4), 1701071 (2018).
24. A. Belabbas and M. Lazoul, "Optical limiter based on two-dimensional nonlinear photonic crystals," Proc. SPIE **9885**, 98851D (2016).
25. M. Xiao, Z. Q. Zhang, and C. T. Chan, "Surface Impedance and Bulk Band Geometric Phases in One-Dimensional Systems," Phys. Rev. X **4**(2), 021017 (2014).
26. C. Li, X. Hu, H. Yang, and Q. Gong, "Unidirectional transmission in 1D nonlinear photonic crystal based on topological phase reversal by optical nonlinearity," AIP Adv. **7**(2), 025203 (2017).
27. J. Ma and Z. Wang, "Band structure and topological phase transition of photonic time crystals," Opt. Express **27**(9), 12914 (2019).
28. A. Yariv and P. Yeh, *Optical Waves in Crystals: Propagation and Control of Laser Radiation* (Wiley, New York, 1984).
29. J. Zak, "Berry's Phase for Energy Bands in Solids," Phys. Rev. Lett. **62**(23), 2747–2750 (1989).
30. W. T. Wang, Z. H. Chen, G. Yang, D. Y. Guan, G. Z. Yang, Y. L. Zhou, and H. B. Lu, "Resonant absorption quenching and enhancement of optical nonlinearity in Au:$BaTiO_3$ composite films by adding Fe nanoclusters," Appl. Phys. Lett. **83**(10), 1983–1985 (2003).
31. V. Ganesh, I. S. Yahia, S. AlFaify, and M. Shkir, "Sn-doped ZnO nanocrystalline thin films with enhanced linear and nonlinear optical properties for optoelectronic applications," J. Phys. Chem. Solids **100**, 115–125 (2017).
32. T. Pencheva and M. Nenkov, "Optical inhomogeneity of $BaTiO_3$ thin films and its correlation with some deposition conditions," Vacuum **58**(2-3), 374–386 (2000).
33. P. Mathey, S. Latour, P. Lompré, P. Jullien, D. Rytz, and B. Salce, "Temperature distribution and thermal-induced defects in photorefractive barium titanate crystals illuminated with intense cw or pulsed laser irradiations," Appl. Phys. B **71**(4), 523–531 (2000).

Optics EXPRESS

34. N. Lameche, S. Bouzid, M. Hamici, M. Boudissa, S. Messaci, and K. Yahiaoui, "Effect of indium doping on the optical properties and laser damage resistance of ZnO thin films," Optik **127**(20), 9663–9672 (2016).
35. Y. Deng, P. Wang, Y. Sun, H. Ming, Q. Zhang, Y. Jiao, and X. Sun, "Nonlinear optical properties of Ag/PMMA nanocomposite polymer film," *2006 International Symposium on Biophotonics, Nanophotonics and Metamaterials* (IEEE, 2006), pp. 373–376.
36. T. D. Krauss and F. W. Wise, "Femtosecond measurement of nonlinear absorption and refraction in CdS, ZnSe, and ZnS," Appl. Phys. Lett. **65**(14), 1739–1741 (1994).
37. R. M. Hussan, Z. F. Mahdi, and R. A. Faris, "Nonlinear Optical Properties of PMMA Composites Using Z-Scan Technique," Iraqi J. Laser **12**, 27–35 (2013).
38. M. Y. Nadeem and W. Ahmed, "Optical Properties of ZnS Thin Films," Turk. J. Phys. **24**(5), 651–659 (2000).
39. P. E. Bath, A. D. Romberger, and P. Brown, "A comparison of Nd:YAG laser damage thresholds for PMMA and silicone intraocular lenses," Invest. Ophthalmol. Vis. Sci. **27**(5), 795–798 (1986).
40. F. Li, G. Liu, L. Du, and R. Zhang, "Comparisons and analyses of the properties of laser-induced damage to SiO_2 and ZnS," J. Mod. Opt. **61**(14), 1158–1163 (2014).
41. S. Dengler, O. Muller, C. Hege, and B. Eberle, "Nonlinear optical effects in colloidal carbon nanohorns—a new optical limiting material," J. Phys. D: Appl. Phys. **49**(36), 365501 (2016).
42. M. D. Zidan, Z. Ajji, A. W. Allaf, and A. Allahham, "Optical limiting behavior of C_{60} doped ethylenepropylenediene polymethylene polymer," Opt. Laser Technol. **42**(4), 600–603 (2010).
43. M. O. Senge, M. Fazekas, E. G. A. Notaras, W. J. Blau, M. Zawadzka, O. B. Locos, and E. M. N. Mhuircheartaigh, "Nonlinear Optical Properties of Porphyrins," Adv. Mater. **19**(19), 2737–2774 (2007).
44. N. Venkatram, D. Narayana Rao, L. Giribabu, and S. Venugopal Rao, "Nonlinear optical and optical limiting studies of alkoxy phthalocyanines in solutions studied at 532 nm with nanosecond pulse excitation," Appl. Phys. B **91**(1), 149–156 (2008).
45. S. Aithal, P. S. Aithal, and G. K. Bhat, "Characteristics of Ideal Optical Limiter and Realization Scenarios Using Nonlinear Organic Materials," Int. J. Adv. Trends Eng. Technol. **1**(1), 73–84 (2016).
46. J. Harris, L. Gai, G. Kubheka, J. Mack, T. Nyokong, and Z. Shen, "Optical limiting properties of 3,5-dithienylenevinylene BODIPY dyes at 532 nm," Chem. - Eur. J. **23**(58), 14507–14514 (2017).
47. F. J. Gonzalez, R. E. Peale, S. Benis, D. Hagan, and E. Van Stryland, "Optical Limiter using Epsilon-Near-Zero Grating," *2019 IEEE Research and Applications of Photonics in Defense Conference (RAPID)* (IEEE, 2019), pp. 1–3.
48. J. Vella, J. Goldsmith, N. Limberopoulos, I. Vitebskiy, E. Makri, and T. Kottos, "Design scalable photonic crystals as reflective optical limiters," *2016 IEEE Photonics Conference (IPC)* (IEEE, 2016), pp. 655–656.
49. B. Y. Soon, J. Haus, M. Scalora, and C. Sibilia, "One-dimensional photonic crystal optical limiter," Opt. Express **11**(17), 2007 (2003).
50. J. W. Elam, Z. A. Sechrist, and S. M. George, "ZnO/Al_2O_3 nanolaminates fabricated by atomic layer deposition: growth and surface roughness measurements," Thin Solid Films **414**(1), 43–55 (2002).
51. O. Lyutakov, I. Goncharova, S. Rimpelova, K. Kolarova, J. Svanda, and V. Svorcik, "Silver release and antimicrobial properties of PMMA films doped with silver ions, nano-particles and complexes," Mater. Sci. Eng., C **49**, 534–540 (2015).
52. C. Inui, Y. Tsuge, H. Kura, S. Fujihara, S. Shiratori, and T. Sato, "Preparation of one-dimensional photonic crystals by sol–gel process for magneto-optical materials," Thin Solid Films **516**(9), 2454–2459 (2008).
53. V. Srikant, E. J. Tarsa, D. R. Clarke, and J. S. Speck, "Crystallographic orientation of epitaxial $BaTiO_3$ films: The role of thermal expansion mismatch with the substrate," J. Appl. Phys. **77**(4), 1517–1522 (1995).
54. M. Esposito, S. Buontempo, A. Petriccione, M. Zarrelli, G. Breglio, A. Saccomanno, Z. Szillasi, A. Makovec, A. Cusano, A. Chiuchiolo, M. Bajko, and M. Giordano, "Fiber Bragg Grating sensors to measure the coefficient of thermal expansion of polymers at cryogenic temperatures," Sens. Actuators, A **189**, 195–203 (2013).
55. L. A. Valdez, M. A. Caravaca, and R. A. Casali, "Ab-initio study of elastic anisotropy, hardness and volumetric thermal expansion coefficient of ZnO, ZnS, ZnSe in wurtzite and zinc blende phases," J. Phys. Chem. Solids **134**, 245–254 (2019).